Electrochemical Characterization of Sulphide Minerals–Halophilic Bacteria Surface Interaction for Bioflotation Applications

González-Poggini, S.; Luque Consuegra, G.; Kracht, W.; Rudolph, M.; Colet-Lagrille, M.;

Originally published:

October 2021

Metallurgical and Materials Transactions B 52(2021)5, 3373-3382

DOI: https://doi.org/10.1007/s11663-021-02267-7

Electrochemical Characterization of Sulfide Minerals-Halophilic Bacteria Surface Interaction for Bioflotation Applications

Sergio González-Poggini[a,b], Guillermo Luque Consuegra[d], Willy Kracht[b,c], Martin Rudolph[d], Melanie Colet-Lagrille[a,b,*]

[a] Department of Chemical Engineering, Biotechnology and Materials, Faculty of Physical and Mathematical Sciences, Universidad de Chile, Beauchef 851, Santiago, Chile

[b] Advanced Mining Technology Centre (AMTC), Faculty of Physical and Mathematical Sciences, Universidad de Chile, Av. Tupper 2007 (AMTC Building), Santiago, Chile

[c] Department of Mining Engineering, Faculty of Physical and Mathematical Sciences, Universidad de Chile, Beauchef 850, Santiago, Chile

[d] Helmholtz-Zentrum Dresden-Rossendorf, Helmholtz Institute Freiberg for Resource Technology Chemnitzer Str. 40, 09599 Freiberg, Germany

[*] corresponding author (email: mcolet@ing.uchile.cl)

Abstract

The effects of halophilic bacteria (*Halobacillus* sp. and *Marinobacter* sp.) on pyrite and chalcopyrite surface oxidation in artificial seawater is studied by electrochemical impedance spectroscopy (EIS) in conjunction with X-ray diffraction (XRD) and cyclic voltammetry analysis (CV), in order to explain the influence of these microorganisms on the minerals floatability. EIS analyses on pyrite electrodes suggest that biomaterial from both bacteria adheres to the mineral surface, which is reinforced by CV experiments as capacitive currents are promoted by both bacteria. Additionally, XRD analyses of pyrite electrodes after immersion in artificial seawater with and without bacteria indicate the formation of hematite on the mineral surface in the presence of *Halobacillus* sp., which together with the adherence of biomaterial could promote the depression of pyrite during flotation. On the other hand, EIS and CV analyses on chalcopyrite electrodes suggest that the adherence of *Halobacillus* sp. and *Marinobacter* sp. to the surface of the mineral have no significant effects on the kinetics of the chalcopyrite oxidation processes. These results together with XRD analyses of the chalcopyrite electrodes after immersion in artificial seawater with and without bacteria suggest that superficial sulphur might have a stronger influence on chalcopyrite flotability than the presence of bacteria.

Keywords: bioflotation, halophilic bacteria, chalcopyrite oxidation, pyrite oxidation, electrochemical impedance spectroscopy

1. Introduction

Chalcopyrite ($CuFeS_2$) is one of the most widely used minerals for copper production processes. It is frequently found associated with iron sulphide minerals such as pyrite, which are considered as gangue and removed by flotation to reduce their concentration during copper minerals processing.[1] In a flotation unit, the ore particles are mixed with water to form a pulp and their surface properties are modified by addition of flotation reagents such as collectors – which increase the hydrophobicity of the target minerals (e.g. chalcopyrite) – and depressants – which decrease the floatability of the unwanted ones (e.g. pyrite) – . Air is sparged into the pulp to produce bubbles, so that the hydrophobic particles adhere to them and are carried up to the surface of the flotation unit to form a froth, which is removed, rinsed and dried to obtain the concentrate.[2]

It is well known that flotation processes are intensive in terms of water consumption and that drinking water resources are increasingly scarce worldwide; consequently, the use of seawater appears to be a sustainable solution to reduce the water footprint of the mining industry, particularly for mine sites close to the seashore. Nowadays, numerous copper sulphide flotation plants in Australia, Canada, Chile and Indonesia operate using seawater.[3,4] However, the implementation of flotation processes using seawater is challenging since surface chemistry phenomena differ to those observed when using fresh water; the saline environment of seawater compresses the electrical double layer in the surface of hydrophobic minerals, resulting in enhancement of the flotability, entrainment and the reduction of bubbles size.[4] In addition, some seawater components (e.g. carbonate/bicarbonate and borate/boric acid) exert a buffering effect in the pulp; this particularly impacts on the lime (pH modifier and pyrite depressant) consumption in Cu-Mo flotation processes, which increases when using seawater.[5]

In the last decades, bioflotation has arisen as an alternative to overcome the difficulties associated with the use of seawater in flotation processes. Bioreagents are less toxic than some of the most common flotation reagents (such as petroleum oils, xanthates, cyanides, and amines) and have proven to be effective collectors, depressants and frothers for a wide selection of minerals, exhibiting high selectivity and specificity under diverse operation conditions.[6–8] In comparison with conventional reagents, the microorganisms (and their associated metabolites) explored for mineral processing are biodegradable and environmentally friendly. However, most of the bioflotation studies to the date are at the laboratory scale; therefore, further research is required on the scaling up of the microorganisms and biomolecules

production methods using genetic engineering and recombinant DNA technologies for the development of highly active and non-pathogenic microorganisms, appropriate for large scale industrial applications.[7] A recent study shows the potential of halophilic bacteria, a group of microorganisms adapted to live in extreme conditions with high salt concentrations, in substitution of lime as the pyrite depressant agent in a flotation process using seawater: the calculated floatability of pyrite is lower than 10% in the presence of *Halobacillus* sp.[9] This previous study was primarily focused on floatability and depression experiments, thus the phenomena associated with the interaction of the mineral surface and the bacteria remain unclear (zeta potential experiments were performed, but inconclusive results were obtained).

The present work investigates the effects of *Halobacillus* sp. and *Marinobacter* sp. on pyrite and chalcopyrite surface oxidation processes occurring when the minerals are immersed in seawater. To accomplish this, electrochemical impedance spectroscopy analysis was conducted using mineral-coated working electrodes and artificial seawater containing *Halobacillus* sp. or *Marinobacter* sp. as electrolyte. Additionally, X-ray diffraction analysis and cyclic voltammetry measurements were performed to complement the results obtained.

2. Experimental

2.1. Pyrite and chalcopyrite electrodes fabrication

Pyrite and chalcopyrite samples used in this study were obtained from Dr. F. Krantz – Reinisches Mineralien Kontor GmbH & Co. KG, Germany. The mineral was first crushed and then dry sieved to obtain fine ground particles. Afterwards, it was ground using a mortar and pestle to obtain a grain size smaller than 37 µm (Tyler mesh 400).

Stainless-steel plates (AISI 316L) were used as conductive supports for the minerals coating. An area of 3 cm^2 on the stainless-steel plates was polished using P1200 sandpaper; the remining area was insulated using a non-conducting varnish (Imp Lacktherm 1303 B, Tintas Weg). The polished area of the stainless-steel plates was covered with a double-sided adhesive conductive carbon tape (3M™ XYZ-Axis Electrically Conductive Tape 9713) and ground mineral was pasted to its surface applying gentle manual pressure to aid the sticking of the particles (this process was repeated twice). Before each experiment, the

so manufactured electrodes were washed with a 6 M HCl aqueous solution to remove superficial oxides and rinsed with deionized water.

2.2. Artificial seawater preparation and microbiological culture

Artificial seawater was prepared following the methodology reported by Kester *et al*., which composition is: 23.93 g L^{-1} NaCl, 10.83 g L^{-1} $MgCl_2$, 4.01 g L^{-1} Na_2SO_4, 1.52 g L^{-1} $CaCl_2$, and 0.68 g L^{-1} KCl (with minor traces of Br, F, and Sr).[10] After preparation, the pH of the solution was adjusted to 8.0 by means of bubbling compressed air for 3 hours.[11–13] The use of artificial seawater aims to provide a reproducible environment to perform experimental work and minimize biological effects. Marine microorganisms are considered to be about 70% of the biomass in the ocean, including bacteria, archaea, viruses and protozoa.[14]

Following that previously reported by Luque Consuegra *et al*. regarding floatability and depression experiments, the halophilic bacteria *Halobacillus* sp. and *Marinobacter* sp. (isolated and characterized by Dr. Götz Haferburg from the Technical University Bergakademie Freiberg) were employed in this study.[9] The bacteria were cultured according to a two-stage method. In the first stage (growing phase), bacteria were cultivated in Halobacillus medium at pH 7.5 for 48 hours in a shaker (100 rpm and 37°C). After incubation, bacterial cells were harvested by centrifugation at 11 000 rpm and 4°C for 15 minutes, rinsed twice with sterilized artificial seawater and finally resuspended in 10 mL of artificial seawater. Control experiments were performed simultaneously to assure sterility. In the second stage, a 5 mL sample of the resuspended bacteria solution was inoculated into 250 mL of sterilized artificial seawater containing peptone/casein (3 g L^{-1}) and yeast extract (5 g L^{-1}). Bacteria were incubated in this medium for 48 hours in a shaker at 100 rpm and 37°C. The growth and concentration of biomass was characterized by optical density analysis using a wavelength of 600 nm (OD600)[15] and cells were harvested within 3 h of reaching the maximum optical density in the medium.[16] Bacterial cells were harvested by centrifugation at 11 000 rpm and 4°C for 15 minutes, rinsed twice with sterilized artificial seawater and finally resuspended in 20 mL of artificial seawater. Finally, this suspension was incubated in a shaker at 100 rpm and 37°C for 1 hour before any experiment.

125 *2.3. X-ray diffraction analysis*

126 The fabricated pyrite and chalcopyrite electrodes were immersed for 60 minutes in artificial seawater in
127 the presence and absence of bacteria. To identify changes in the crystallinity and composition of the
128 electrodes, samples were characterized immediately after these experiments by X-ray diffraction (XRD)
129 analysis using a Bruker D8 Advance diffractometer with $Cu_{K\alpha}$ radiation (λ = 0.15406 nm) and working at
130 30 kV / 40 mA in a scanning angle (2θ) range from 20° to 70° with a step size of 0.02°.

131 *2.4. Electrochemical measurements*

132 The oxidation of pyrite and chalcopyrite in artificial seawater in the presence and absence of bacteria was
133 studied by cyclic voltammetry (CV) and electrochemical impedance spectroscopy (EIS) analyses, using a
134 Gamry Reference 3000 potentiostat/galvanostat/ZRA. For this purpose, a 100 mL glass cell was filled
135 with an electrolyte comprised of 80 mL of artificial seawater and 3 mL of resuspended bacteria solution
136 when required (cell concentration of ca. 58.6 g L^{-1} and 54.8 g L^{-1} for *Halobacillus* sp. and *Marinobacter*
137 sp., respectively). The pyrite/chalcopyrite electrodes fabricated were used as working electrodes, while a
138 platinum wire and an Ag/AgCl (3 M KCl) electrode were used as counter electrode and reference,
139 respectively[1]. All experiments were conducted at 25°C and repeated at least three times to confirm the
140 reproducibility of the results.

141 CV measurements were performed between -0.3 V and 0.3 V for pyrite electrodes and between -0.5 V
142 and 0.5 V for chalcopyrite electrodes, both at a scan rate of 4 mV s^{-1} with a step size of 1 mV for one
143 cycle.

144 For EIS measurements, a perturbation signal with 10 mV AC amplitude around the open-circuit potential
145 (OCP) was applied to the working electrode. Frequencies analysed were between 400 kHz and 0.1 Hz for
146 pyrite electrodes and between10 kHz and 0.1 Hz for chalcopyrite electrodes, with 10 points per decade
147 each. The pyrite or chalcopyrite electrodes were immersed for 60 minutes in the electrolyte solution (with
148 or without bacteria as it corresponds) and EIS measurements were performed every 15 minutes.

149

[1] All the potentials presented in this work are referred to this electrode, unless noted otherwise.

3. Results and discussion

3.1. XRD analysis of pyrite and chalcopyrite electrodes

The fabricated pyrite and chalcopyrite electrodes were immersed for 60 minutes in artificial seawater in the presence and absence of bacteria. XRD patterns of pyrite before and after the immersion experiments are depicted in Figure 1. As can be seen, the diffractogram obtained for the pyrite electrode before immersion (Figure 1(a)) shows typical peaks for pyrite at 28.55°, 33.07°, 37.10°, 40.79°, 47.45°, 56.29°, 59.02°, 61.70° and 64.29° (PDF# 01-071-1680), which are also clearly distinguished in Figure 1(b), 1(c) and 1(d). The peaks located at 44.58° and 52.92° are associated with the Ti support used during XRD analyses. The electrode immersed in seawater containing *Halobacillus* sp. (Figure 1(c)) shows an additional peak at 25.46°, which can be associated to hematite according to previous studies on pyrite oxidation in alkaline media.[17] Additionally, a quantification analysis was performed from the diffractograms of pyrite electrodes immersed in seawater containing *Halobacillus* sp., which suggests a content of 13% hematite and 87% pyrite (not considering the peaks associated with the Ti support). Consequently, the calculated rate of hematite formation is 0.175 mg hematite h^{-1} (g bacteria)$^{-1}$.

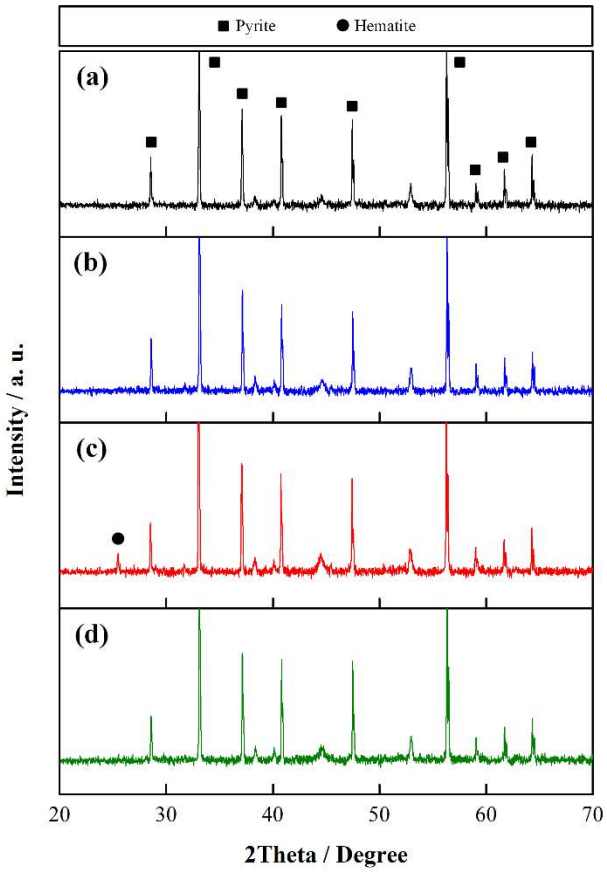

Fig. 1. XRD patterns of pyrite electrodes (a) before immersion experiments, and after 60 minutes of immersion in: (b) artificial seawater, (c) artificial seawater with *Halobacillus* sp., (d) artificial seawater with *Marinobacter* sp.

The diffractograms of chalcopyrite electrodes before and after the immersion experiments are shown in Figure 2. The XRD pattern for chalcopyrite electrodes before the immersion experiments (Figure 2(a)) exhibits the peaks associated to chalcopyrite at 29.44°, 33.93°, 38.28°, 48.70°, 49.10°, 52.96°, 57.89° and 58.57° (PDF# 00-037-0471), and the presence of quartz as an impurity (peaks at 26.56° and 40.14°, PDF# 01-085-1780). These peaks are also distinguished in Figure 2(b), 2(c) and 2(d) for the samples after immersion experiments, together with the presence of a peak at 31.74° that can be associated with elemental sulphur.[18] Chalcopyrite electrodes before immersion showed a 98% content of chalcopyrite and a 2% of quartz.

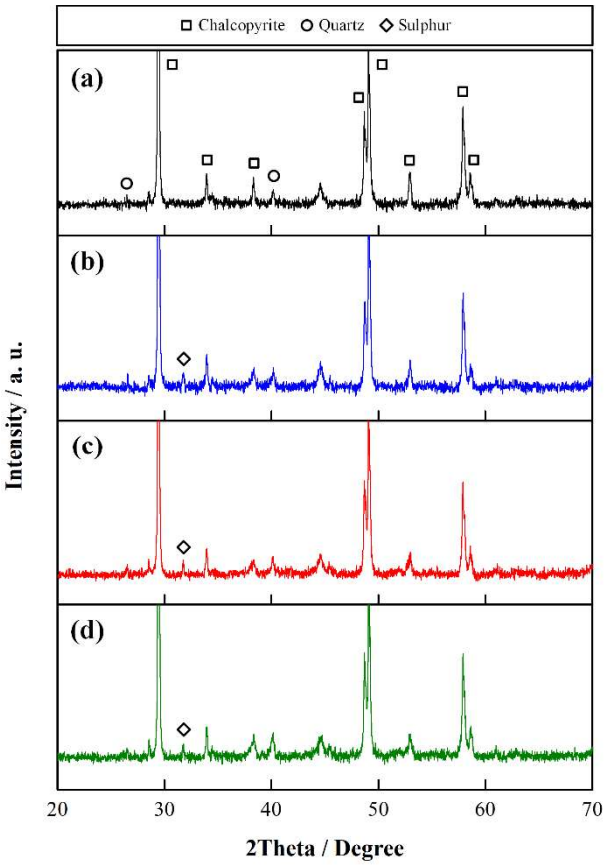

Fig. 2. XRD patterns of chalcopyrite electrodes (a) before immersion experiments, and after 60 minutes of immersion in: (b) artificial seawater, (c) artificial seawater with *Halobacillus* sp., (d) artificial seawater with *Marinobacter* sp.

3.2. Cyclic voltammetries in artificial seawater with and without bacteria

Figure 3 shows the voltammograms obtained for pyrite electrodes in artificial seawater, in the presence and absence of bacteria. As can be seen, the voltammogram for pyrite electrodes in artificial seawater is similar to those reported for pyrite in alkaline media after a pre-treatment with acid.[19] The presence of *Marinobacter* sp. in the electrolyte generates a higher current density at the anodic potential limit (0.3 V) compared to that measured in pure artificial seawater, with the distinguishing characteristic of large capacitive currents. This increase in current density has been observed in the presence of other bacteria (*P. aeruginosa*) and it has been attributed to an electrochemical interaction between the bacterial surface-associated molecules and the surface of the electrode.[20] Furthermore, it is known from the literature that *Marinobacter* sp. synthesise ferritins, proteins responsible for iron oxidation and storage: ferrous ions are translocated to ferroxidation centres where, in the presence of hydrogen peroxide or molecular oxygen, are oxidized.[21] Recent studies have detected that ferritins are capable of oxidizing iron even in anoxic environments, through electron transfer reactions from the aqueous Fe(II) to the solid ferric mineral.[22]

This capacity of ferritins for iron oxidation might possibly have contributed to the increase in the current density observed in the voltammogram for pyrite in the presence of *Marinobacter* sp.

On the other hand, the presence of *Halobacillus* sp. in the electrolyte produces a maximum anodic current density similar to that measured for pyrite in pure artificial seawater. However, capacitive currents can be noticed after the oxidation of the mineral, which could be ascribed to adsorption of exopolysaccharides or bacterial cells. The component generating this capacitive behaviour is not clear yet but might lead to the formation of the hematite phase detected in the XRD analysis (Figure 1(c)).

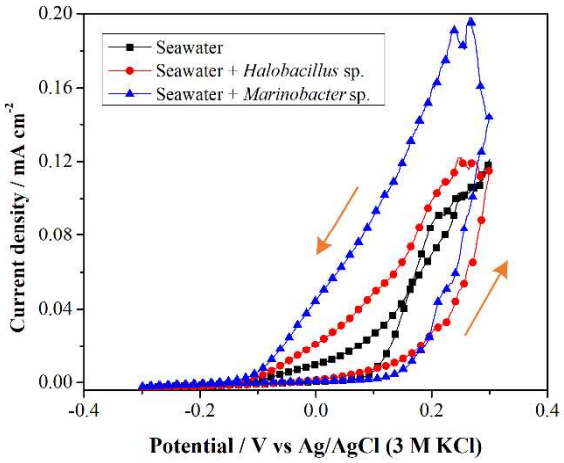

Fig. 3. Voltammograms obtained in artificial seawater for pyrite electrodes in the presence and absence of bacteria.

Figure 4 shows the voltammograms obtained in artificial seawater in the presence and absence of bacteria for chalcopyrite electrodes. It can be observed that the maximum anodic current density is similar in all experiments. However, in the presence of bacteria small capacitive currents can be noticed which could be related to the presence of molecules or bacterial cells in the surface of the mineral.[16,20]

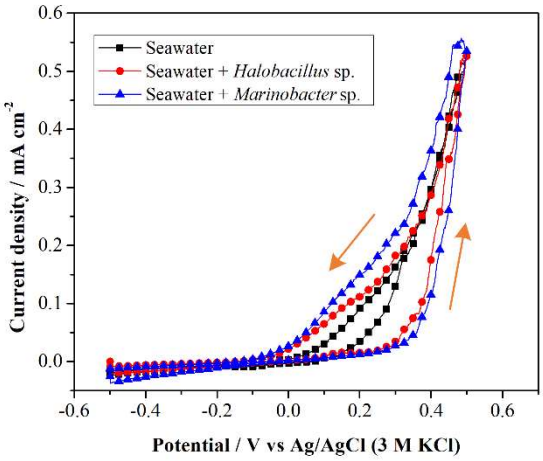

206

207 **Fig. 4**. Voltammograms obtained in artificial seawater for chalcopyrite electrodes in the presence and absence of
208 bacteria.
209

210 *3.3. Electrochemical impedance spectroscopy in artificial seawater with and without bacteria*

211 The phenomena taking place on the surface of the pyrite and chalcopyrite electrodes immersed in
212 artificial seawater with and without bacteria were modelled using equivalent circuits. The equivalent
213 circuit 1 (Figure 5(a)) is proposed to model the EIS experimental data obtained for pyrite electrodes: $R_{p,1}$
214 represents the solution resistance, $R_{p,2}$ is the charge transfer resistance, $CPE_{p,1}$ is a constant phase element
215 which describes the double-layer capacitance of the solution-electrode interface,[23] $C_{p,1}$ is the biomaterial
216 capacitance and $R_{p,3}$ is the biomaterial resistance (generated by bacteria and biomolecules).[24–27] The
217 equivalent circuit 2 (Figure 5(b)) is proposed to model the EIS experimental data obtained for
218 chalcopyrite electrodes, considering that a part of the electrode surface is covered by an adherent layer
219 probably composed by sulphur, hydroxides, biomolecules and cells as discussed below.[27] In this
220 equivalent circuit, $R_{c,1}$ represents the solution resistance, $CPE_{c,1}$ is a constant phase element which
221 describes the double-layer capacitance of the solution-electrode interface, $CPE_{c,2}$ and $R_{c,2}$ are associated
222 to the layer of sulphur, hydroxides and biomolecules/cells and $R_{c,3}$ is the charge transfer resistance.

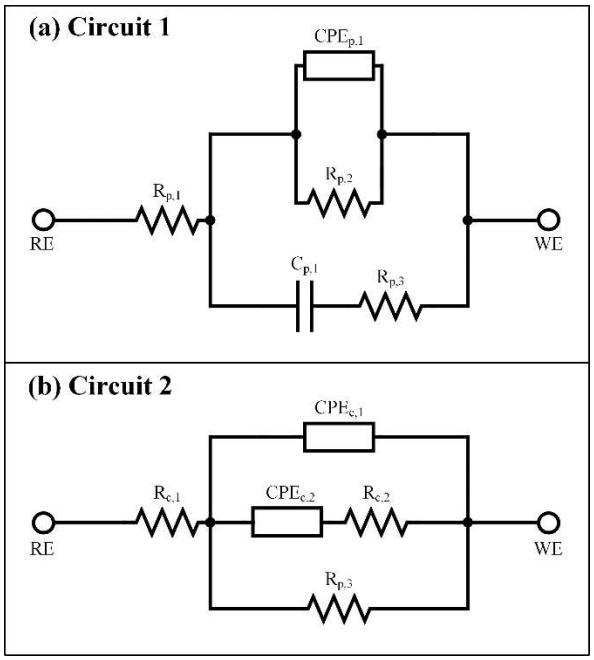

Fig. 5. Equivalent circuits describing the electrochemical interaction between: (a) pyrite and the electrolyte and (b) chalcopyrite and the electrolyte.

The results of EIS measurements for pyrite electrodes in the presence and absence of bacteria are presented in Figure 6 in the form of Nyquist plots. The impedance data were tested using Kramers-Kronig transforms (KKTs) for validation. Details on the formulation of KKTs can be found elsewhere.[28,29] The results obtained suggest that the impedance data were valid since the maximum residual error for all experiments is not higher than 1.3%. Moreover, the sum of quadratic deviations between the EIS experimental and calculated KKT data (Goodness of Fit, GoF) shows an average value of 22.5 x 10^{-6}. The EIS data was fitted to circuit 1 using the Gamry Echem Analyst software v6.23, applying simplex method in the curve fitting toolbox. The values of the fitted parameters associated with each circuit element can be found in Appendix A. Supplementary data (Table A1, A2 and A3). The GoF of experimental and simulated data display an average value of 5.39 x 10^{-4}, suggesting that the proposed circuit is suitable for explaining the EIS spectra. An example of the results obtained by fitting the equivalent circuit 1 is shown in Figure 6(d).

Pyrite oxidation experiments are typically performed in acid environments where pyrite reacts with Fe^{3+} ions in the solution resulting in the solubilization of pyrite to Fe^{2+}.[30] In this research the environment is alkaline since the pH value of the artificial seawater was adjusted to 8.0 (see section 2.2). Under this condition, Fe^{3+} ions are insoluble and sulphide minerals are oxidised by dissolved molecular oxygen, resulting in the formation of soluble sulphate and amorphous iron oxyhydroxides.[31] Nicholson *et al.*

established an stoichiometric equation for pyrite oxidation in circumneutral solutions with iron oxyhydroxides forming as a product:[32]

$$FeS_{2(s)} + 3.75O_{2(aq)} + 3.5H_2O_{(l)} \rightarrow Fe(OH)_{3(s)} + 2SO^{2-}_{4(aq)} + 4H^{+}_{(aq)} \quad (1)$$

The formation of iron oxyhydroxides on the surface of pyrite is expected to result in a reduced available surface for charge-transfer reactions and therefore, an increase in the charge-transfer resistance, $R_{p,2}$. From Figure 7a, it can be seen that in all conditions a continuous increase of $R_{p,2}$ is obtained.

Regarding $R_{p,1}$ values in the presence and absence of bacteria in the electrolyte, it was obtained that the presence of bacteria slightly reduces the value of the solution resistance at any time of immersion; this behaviour could be associated with addition of the bacterial sample, which contains metabolites from the bacteria. The $CPE_{p,1}$ component is related with the capacitance of the electrode | electrolyte interface: $n_{p,1}$ values show a relatively steady capacitive behaviour (values between 0.7 and 0.9), almost independent of the presence of bacteria. The deviation from a value of 1 (capacitor) is attributed to the surface heterogeneities and roughness since values between 0.5 and 1 can be considered a capacitive behaviour modified by the heterogeneity of the surface.[27]

Luque Consuegra *et al.* performed bacteria adherence experiments on pyrite obtaining that *Halobacillus* sp. presented higher adhesion to the sulphide surface than *Marinobacter* sp.[9] In EIS experiments the attachment of the biomaterial to the surface of pyrite can be characterized by $C_{p,1}$ and $R_{p,3}$. The $C_{p,1}$ values obtained in the presence of *Halobacillus* sp. are in average ca. 31% higher compared to these obtained in the presence of *Marinobacter* sp. On the other hand, as shown in Figure 7(b), $R_{p,3}$ initially increases over time to reach its maximum value between 30 to 45 minutes with a subsequent decrease. This behaviour could be ascribed to an increase in the number of bacteria attached to the electrode surface, which results in an increase of $R_{p,3}$. However, after a certain time, bacterial cells begin to have contact with each other generating an increase in the density of the resistance connected in parallel, which finally decreases the total bacterial resistance.

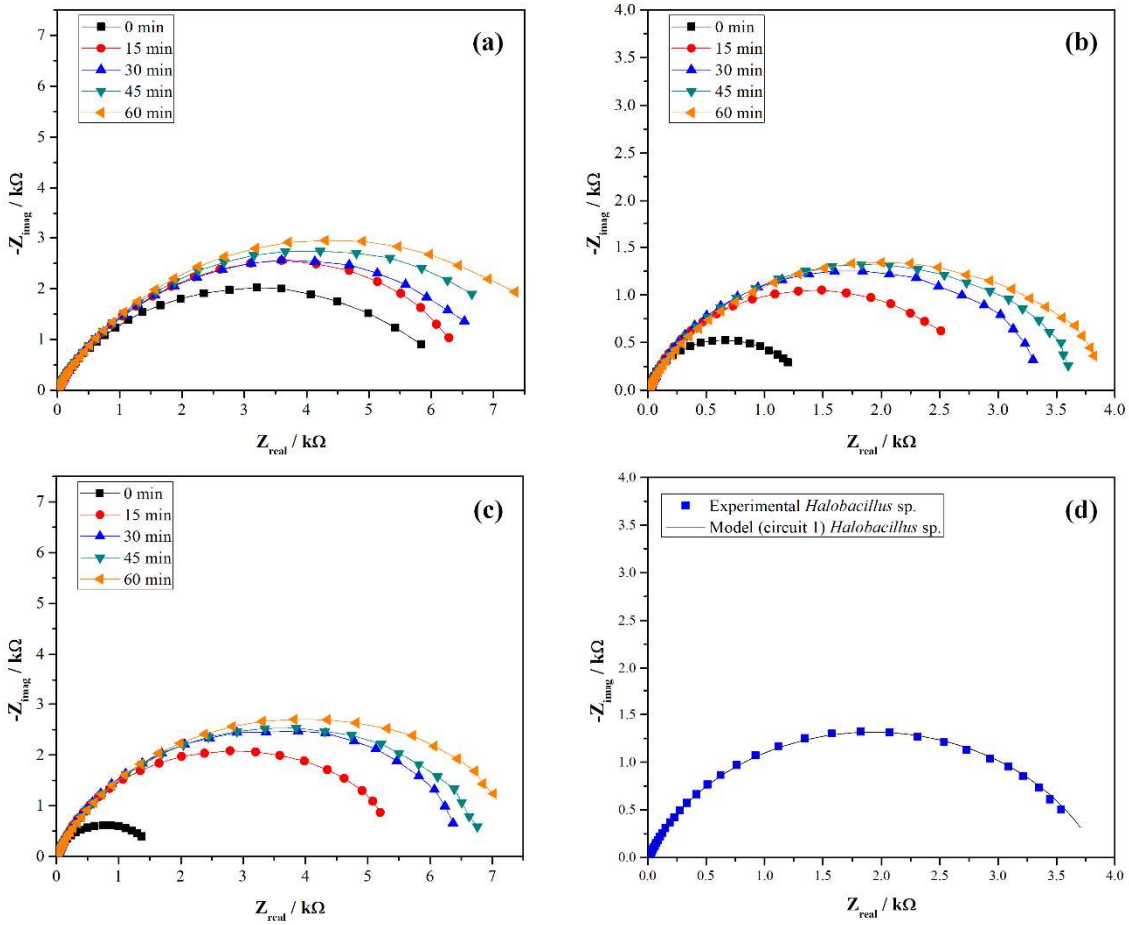

Fig. 6. Nyquist plots for pyrite electrodes at different immersion times in: (a) artificial seawater, (b) artificial seawater with *Halobacillus* sp., and (c) artificial seawater with *Marinobacter* sp. (d) example of the result obtained by fitting the equivalent circuit 1 to EIS data.

Previous studies on pyrite floatability in the presence of halophilic bacteria have reported that the floatability of this sulphide can be drastically reduced to below 10% in the presence of *Halobacillus* sp., while no significant depression was obtained in the presence of *Marinobacter* sp.[9] In this research, CV experiments show capacitive currents for both bacteria indicating that both biomaterials adhere to the surface of pyrite. In addition, EIS analyses reinforce that the biomaterial of both bacteria adheres to the mineral surface ($R_{p,3}$) with *Halobacillus* sp. showing a stronger interaction. Furthermore, when analysing the electrodes by XRD only the experiments in the presence of *Halobacillus* sp. promoted the formation of a hematite phase on the surface of the mineral, which together with the adherence of biomaterial could be responsible for the depression of pyrite[9] considering that recent studies have reported that polysaccharides act as depressants of hematite by absorbing on its surface, making it hydrophilic.[33]

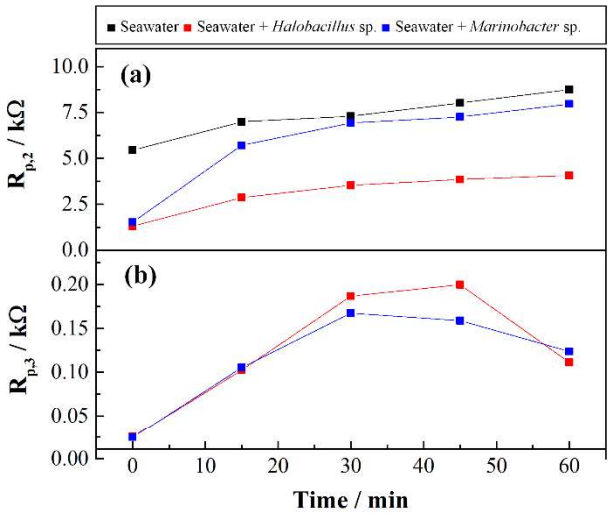

Fig. 7. Time-dependence of equivalent circuit model resistances obtained for pyrite electrodes immersed in seawater without or with bacteria: (a) $R_{p,2}$ (charge transfer resistance) and (b) $R_{p,3}$ (biomaterial resistance).

The results of EIS measurements for chalcopyrite electrodes in the presence and absence of bacteria are presented in Figure 8. The Nyquist plots of chalcopyrite electrodes at different immersion times are similar in appearance exhibiting two capacitive components deviated from an ideal semicircle. KKT analyses of the obtained EIS spectra indicate that the experimental data is valid presenting a maximum residual error of 1.7% and an average GoF of 29.1 x 10^{-6}. The resulting impedance spectroscopy was fitted to the equivalent circuit 2 using the Gamry Echem Analyst software v6.23. The parameters fitted for the experimental results can be found in Appendix A. Supplementary data (Table A4, A5 and A6).

An empirical reaction for chalcopyrite oxidation in circumneutral artificial seawater has been proposed by Knight *et al*., which suggests the formation of iron oxyhydroxide as product:[31]

$$CuFeS_{2(s)} + 8.5O_{2(aq)} + 5H_2O_{(l)} \rightarrow CuO_{(s)} + Fe(OH)_{3(s)} + 4SO^{2-}_{4(aq)} + 8H^{+}_{(aq)} \quad (2)$$

The formation of amorphous iron oxyhydroxide on the surface of the chalcopyrite electrode, along with sulphur, is expected to cause an increase in the charge-transfer resistance. This is corroborated by the results presented in Figure 9(a) for the time-dependence of $R_{c,3}$, which is enhanced by the presence of bacteria in seawater. The increase of charge-transfer resistance in the presence of bacteria could be explained by the attachment of biomaterial to the electrode surface, which is consistent with the increased capacitive behaviour of the current densities observed in the voltammograms shown in Figure 4 for chalcopyrite electrodes immersed in seawater containing *Halobacillus* sp. and *Marinobacter* sp. However, the resistance associated with the attachment of biomaterial to the electrode ($R_{c,2}$) shows a

decreasing behaviour over time for experiments using bacteria in seawater, which could be explained by changes on the chalcopyrite surface composition as a result of reaction (2) promoting detachment or reorganization of biomolecules and bacterial cells.

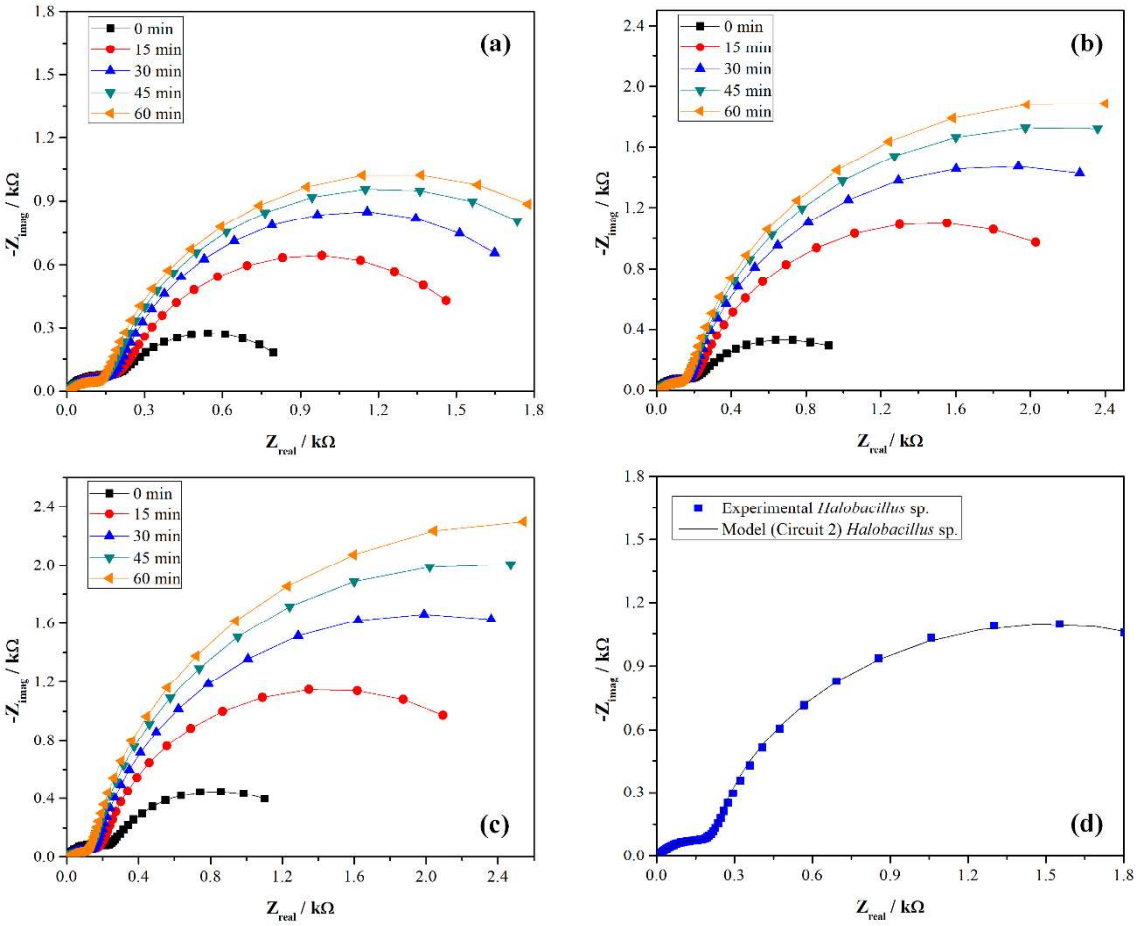

Fig. 8. Nyquist plots for chalcopyrite electrodes at different immersion times in: (a) artificial seawater, (b) artificial seawater with *Halobacillus* sp., and (c) artificial seawater with *Marinobacter* sp. (d) example of the result obtained by fitting the equivalent circuit 2 to the EIS data.

The behaviour of the solution resistance ($R_{c,1}$) over time is shown in Figure 9(b). A slight decrease (5% on average) of $R_{c,1}$ can be observed after 15 minutes of immersion in all experiments, which could be explained by the addition of ionic species such as SO_4^{2-} and H^+ to the electrolyte, in accordance with reaction (2). In addition, the $CPE_{c,2}$ component (sulphur/oxides and biomolecules/cells layers resistance) displays n values with a relatively steady capacitive behaviour (values between 0.8 and 1), almost independent of the presence of bacteria. On the other hand, and similarly to pyrite, the $CPE_{c,1}$ component (double-layer capacitance of the solution-electrode interface) shows n values between 0.5 and 1.0, which could be explained by surface heterogeneity or porosity.[34]

Luque Consuegra *et al*. found that natural flotation of chalcopyrite was scarcely improved in the presence of *Halobacillus* sp. or *Marinobacter* sp.[9] This is in good agreement with the EIS and CV analyses discussed previously, which suggest that the adherence of *Halobacillus* sp. and *Marinobacter* sp. to the surface of the mineral (electrode) has no significant effects on the kinetics of the chalcopyrite oxidation processes (analogous oxidation current densities than those obtained using pure seawater and increasing charge transfer resistances over time). Based on that and the XRD analysis of the chalcopyrite electrode surface after immersion experiments in the presence and absence of bacteria shown in Figure 2, it is thought that chalcopyrite floatability is not importantly influenced by the microorganisms but mainly due to the presence of surface oxides and elemental sulphur formed by contact of the mineral with seawater, which is in good agreement with results reported previously by other authors.[35,36]

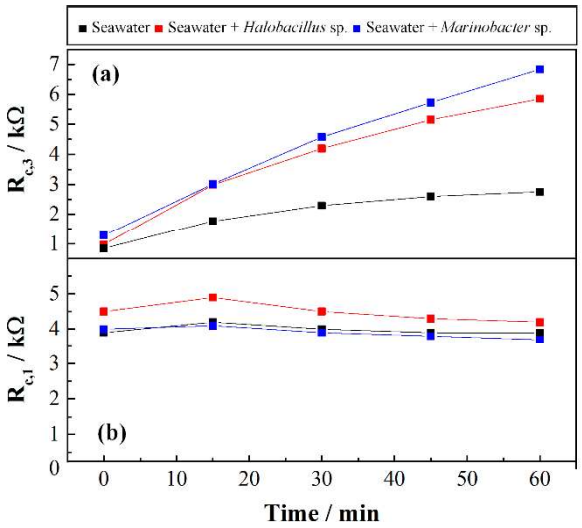

Fig. 9. Time-dependence of equivalent circuit model resistances obtained for chalcopyrite electrodes immersed in seawater without and with bacteria: (a) $R_{c,3}$ (charge transfer resistance) and (b) $R_{c,1}$ (solution resistance).

4. Conclusions

The effects of *Halobacillus* sp. and *Marinobacter* sp. (halophilic bacteria) on pyrite and chalcopyrite surface oxidation processes in artificial seawater were investigated by electrochemical impedance spectroscopy (EIS). EIS analyses on pyrite electrodes showed that the biomaterial of both bacteria adheres to the mineral surface, which was also detected during the cyclic voltammetry (CV) experiments as capacitive currents are promoted by the presence of both bacteria. Additionally, XRD analyses of pyrite electrodes immersed in seawater with and without bacteria showed that in the presence of *Halobacillus* sp. a hematite phase is generated on the surface of the mineral which together with the

favoured adherence of biomaterial could be the responsible for the depression of pyrite reported in previous flotation studies. On the other hand, EIS and CV analyses for chalcopyrite electrodes suggest that the adherence of *Halobacillus* sp. and *Marinobacter* sp. to the surface of the mineral have no significant effects on the kinetics of the chalcopyrite oxidation processes. Furthermore, XRD analysis of the chalcopyrite electrode surface after immersion experiments showed the presence of elemental sulphur formed by contact of the mineral with seawater, which might have a stronger influence on its floatability than the presence of bacteria.

Acknowledgments

The authors are grateful for the financial support from the CONICYT-BMBF international cooperation project BMBF150026: "Bioflotation of Sulfides in Seawater: Evaluation of Potential Application of Biocomponents in Copper Ore Processing with Seawater (BS2)" and the CONICYT-PIA project AFB180004. Also, the authors thank Dr. Götz Haferburg from the Technical University Bergakademie Freiberg (TUBAF) for his collaboration on the isolation and initial characterization of the bacteria strains.

References

1 C. Owusu, S. Brito, W. Skinner, J. Addai-mensah, and M. Zanin: *Miner. Eng.*, 2014, vol. 55, pp. 87–95.

2 X.-H. Wang and K.S. Eric Forssberg: *Int. J. Miner. Process.*, 1991, vol. 33, pp. 275–90.

3 S.K. Behera and A.F. Mulaba-Bafubiandi: *Miner. Eng.*, 2019, vol. 131, pp. 336–41.

4 R.I. Jeldres, L. Forbes, and L.A. Cisternas: *Miner. Process. Extr. Metall. Rev.*, 2016, vol. 37, pp. 369–84.

5 R.M. Pytkowicz and E. Atlas: *Limnol. Oceanogr.*, 1975, vol. 20, pp. 222–9.

6 P. Patra and K. Natarajan: *Int. J. Miner. Process.*, 2008, vol. 88, pp. 53–8.

7 S.K. Behera and A.F. Mulaba-Bafubiandi: *Miner. Process. Extr. Metall. Rev.*, 2017, vol. 38, pp. 96–105.

8 F. San Martín, W. Kracht, and T. Vargas: *Miner. Eng.*, 2018, vol. 117, pp. 127–31.

9 G. Luque Consuegra, S. Kutschke, M. Rudolph, and K. Pollmann: *Miner. Eng.*, 2020, vol. 145, p. 106062.

10 D.R. Kester, I.W. Duedall, D.N. Connors, and R.M. Pytkowicz: *Limnol. Oceanogr.*, 1967, vol. 12, pp. 176–9.

11 C.Y. Chen and E.G. Durbin: *Mar. Ecol. Prog. Ser.*, 1994, vol. 109, pp. 83–94.

12 S. Gao, Q. Sun, Y. Tao, X. Wang, W. Li, L. Huan, M. Wu, and G. Wang: *J. Exp. Mar. Bio. Ecol.*, 2016, vol. 475, pp. 144–53.

13 I.S. Semesi, J. Kangwe, and M. Björk: *Estuar. Coast. Shelf Sci.*, 2009, vol. 84, pp. 337–41.

14 Y.M. Bar-On, R. Phillips, and R. Milo: *Proc. Natl. Acad. Sci. U. S. A.*, 2018, vol. 115, pp. 6506–11.

15 E.G. Biesta-Peters, M.W. Reij, H. Joosten, L.G.M. Gorris, and M.H. Zwietering: *Appl. Environ. Microbiol.*, 2010, vol. 76, pp. 1399–405.

16 E. Marsili, J.B. Rollefson, D.B. Baron, R.M. Hozalski, and D.R. Bond: *Appl. Environ. Microbiol.*, 2008, vol. 74, pp. 7329–37.

17 C.L. Caldeira, V.S.T. Ciminelli, A. Dias, and K. Osseo-Asare: *Int. J. Miner. Process.*, 2003, vol. 72, pp. 373–86.

18 D. Bevilaqua, A.L.L.C. Leite, O. Garcia, and O.H. Tuovinen: *Process Biochem.*, 2002, vol. 38, pp. 587–92.

19 E. Ahlberg, K.S.E. Forssberg, and X. Wang: *J. Appl. Electrochem.*, 1990, vol. 20, pp. 1033–9.

20 J. Kang, T. Kim, Y. Tak, J.H. Lee, and J. Yoon: *J. Ind. Eng. Chem.*, 2012, vol. 18, pp. 800–7.

21 E.C. Theil, T. Tosha, and R.K. Behera: *Acc. Chem. Res.*, 2016, vol. 49, pp. 784–91.

22 D. Penas, A.S. Pereira, and P. Tavares: *Angew. Chemie Int. Ed.*, 2019, vol. 58, pp. 1013–8.

23 W.H. Mulder, J.H. Sluyters, T. Pajkossy, and L. Nyikos: *J. Electroanal. Chem.*, 1990, vol. 285, pp. 103–15.

24 S.Y. Shi, Z.H. Fang, and J.R. Ni: *Electrochem. Commun.*, 2005, vol. 7, pp. 1177–82.

25 S. Deng and G. Gu: *Electrochim. Acta*, 2018, vol. 287, pp. 106–14.

26 M.C. Romero, G. Ramos, I. González, and F. Ramírez: *Appl. Biochem. Biotechnol.*, DOI:10.1007/s12010-020-03386-8.

27 D. Bevilaqua, I. Diéz-Perez, C.S. Fugivara, F. Sanz, A. V. Benedetti, and O. Garcia: *Bioelectrochemistry*, 2004, vol. 64, pp. 79–84.

28 B. Boukamp: *Solid State Ionics*, 1993, vol. 62, pp. 131–41.

29 M. Schönleber and D. Klotz: *Electrochim. Acta*, 2014, vol. 131, pp. 20–7.

30 C. Heidel, M. Tichomirowa, and M. Junghans: *Chem. Geol.*, 2013, vol. 342, pp. 29–43.

31 R.D. Knight, S. Roberts, and M.J. Cooper: *Appl. Geochemistry*, 2018, vol. 90, pp. 63–74.

32 R. V. Nicholson, R.W. Gillham, and E.J. Reardon: *Geochim. Cosmochim. Acta*, 1988, vol. 52, pp. 1077–85.

33 K. Shrimali, V. Atluri, Y. Wang, S. Bacchuwar, X. Wang, and J.D. Miller: *J. Colloid Interface Sci.*, 2018, vol. 524, pp. 337–49.

34 P. Velásquez, H. Gómez, D. Leinen, and J.R. Ramos-Barrado: *Colloids Surfaces A Physicochem. Eng. Asp.*, 1998, vol. 140, pp. 177–82.

35 J.R. Gardner and R. Woods: *Int. J. Miner. Process.*, 1979, vol. 6, pp. 1–16.

36 W. Tolley, D. Kotlyar, and R.. Van Wagoner: *Miner. Eng.*, 1996, vol. 9, pp. 603–37.

Appendix A. Supplementary data

Table A1. Impedance parameters obtained for pyrite electrodes in the absence of bacteria using circuit 1 for different immersion times.

Immersion time / min	$R_{p,1}$ / Ω	$R_{p,2}$ / Ω	$Yo_{(p,1)}$ / 10^{-5} S $s^{np,1}$	$n_{p,1}$	$C_{p,1}$ / µF	$R_{p,3}$ / Ω	Goodness of Fit / 10^{-4}
0	5.82	5442	3.40	0.80	–	–	26.5
15	8.37	6999	2.72	0.78	–	–	10.0
30	8.42	7305	2.78	0.77	–	–	7.18
45	8,33	8019	2.86	0.76	–	–	5.77
60	8.08	8746	2.90	0.75	–	–	8.17

Table A2. Impedance parameters obtained for pyrite electrodes in the presence of *Halobacillus* sp. using circuit 1 for different immersion times.

Immersion time / min	$R_{p,1}$ / Ω	$R_{p,2}$ / Ω	$Yo_{(p,1)}$ / 10^{-5} S $s^{np,1}$	$n_{p,1}$	$C_{p,1}$ / µF	$R_{p,3}$ / Ω	Goodness of Fit / 10^{-4}
0	5.67	1303	3.47	0.84	4.60	25.72	2.53
15	7.79	2868	2.84	0.80	1.57	102.4	4.03
30	7.89	3531	3.00	0.78	0.98	186.8	3.74
45	7.48	3854	3.42	0.76	0.66	199.7	1.35
60	6.70	4067	3.85	0.73	0.66	111.2	0.57

Table A3. Impedance parameters obtained for pyrite electrodes in the presence of *Marinobacter* sp. using circuit 1 for different immersion times.

Immersion time / min	$R_{p,1}$ / Ω	$R_{p,2}$ / Ω	$Yo_{(p,1)}$ / 10^{-5} S $s^{np,1}$	$n_{p,1}$	$C_{p,1}$ / µF	$R_{p,3}$ / Ω	Goodness of Fit / 10^{-4}
0	5.62	1534	3.78	0.86	3.98	25.0	1.27
15	8.08	5713	2.76	0.80	1.08	105.3	2.54
30	7.94	6928	2.88	0.78	0.66	167.2	4.74
45	7.56	7256	3.08	0.76	0.53	158.9	1.69
60	7.06	7968	3.27	0.75	0.55	123.7	0.71

Table A4. Impedance parameters obtained for chalcopyrite electrodes in the absence of bacteria using circuit 2 for different immersion times.

Immersion time / min	$R_{c,1}$ / Ω	$R_{c,2}$ / Ω	$Yo_{c,1}$ / 10^{-4} S $s^{nc,1}$	$n_{c,1}$	$Yo_{c,2}$ / 10^{-4} S $s^{nc,2}$	$n_{c,2}$	$R_{c,3}$ / Ω	Goodness of Fit / 10^{-3}
0	3.9	–	–	–	0.76	0.72	852.3	4.61
15	4.2	–	–	–	1.20	0.62	1770	3.11
30	4.0	–	–	–	1.17	0.61	2290	3.45
45	3.9	–	–	–	1.17	0.61	2598	3.76
60	3.9	–	–	–	1.17	0.61	2748	3.71

458 **Table A5.** Impedance parameters obtained for chalcopyrite electrodes in the presence of *Halobacillus* sp. using
459 circuit 2 for different immersion times.

Immersion time / min	$R_{c,1}$ / Ω	$R_{c,2}$ / Ω	$Yo_{c,1}$ / 10^{-4} S $s^{n_{c,1}}$	$n_{c,1}$	$Yo_{c,2}$ / 10^{-4} S $s^{n_{c,2}}$	$n_{c,2}$	$R_{c,3}$ / Ω	Goodness of Fit / 10^{-3}
0	4.5	342	3.46	0.91	0.82	0.71	970.7	2.18
15	4.9	311.3	2.96	0.95	1.33	0.60	2983	1.04
30	4.5	257.8	2.92	0.95	1.42	0.59	4190	1.50
45	4.3	233.8	2.87	0.94	1.46	0.58	5154	1.67
60	4.2	216.8	2.88	0.94	1.46	0.59	5852	2.28

460

461 **Table A6.** Impedance parameters obtained for chalcopyrite electrodes in the presence of *Marinobacters* sp. using
462 circuit 2 for different immersion times.

Immersion time / min	$R_{c,1}$ / Ω	$R_{c,2}$ / Ω	$Yo_{c,1}$ / 10^{-4} S $s^{n_{c,1}}$	$n_{c,1}$	$Yo_{c,2}$ / 10^{-4} S $s^{n_{c,2}}$	$n_{c,2}$	$R_{c,3}$ / Ω	Goodness of Fit / 10^{-3}
0	4.0	336.5	3.39	0.91	4.28	0.76	1283	4.32
15	4.1	217.5	3.51	0.90	6.01	0.67	3012	3.76
30	3.9	170.0	3.62	0.88	6.08	0.67	4575	4.38
45	3.8	142.6	3.54	0.89	6.57	0.66	5730	4.92
60	3.7	133.4	3.41	0.89	6.94	0.66	6832	5.38

463

464